Biol. **12**, 1879 (1992); B. C. Laurent, X. Yang, M. Carlson, *ibid.*, p. 1893.
43. I. Okabe *et al.*, *Nucleic Acids Res.* **20**, 4649 (1992).
44. J. A. Kennison and J. W. Tamkun, *Proc. Natl. Acad. Sci. U.S.A.* **85**, 8136 (1988).
45. R. Paro, *Trends Genet.* **6**, 416 (1990).
46. _____ and D. S. Hogness, *Proc. Natl. Acad. Sci. U.S.A.* **88**, 263 (1991).
47. S. Messmer, A. Franke, R. Paro, *Genes Dev.* **6**, 1241 (1992).
48. D. Moazed, personal communication.
49. R. S. Sikorski and P. Hieter, *Genetics* **122**, 19 (1989).
50. S. Green *et al.*, *Nature* **320**, 134 (1986).
51. L. Guarente and T. Mason, *Cell* **32**, 1279 (1983).
52. R. Brent and M. Ptashne, *Nature* **312**, 612 (1984).
53. B. C. Laurent, M. A. Treitel, M. Carlson, *Mol. Cell. Biol.* **10**, 5616 (1990).
54. F. Estruch and M. Carlson, *ibid.* **10**, 2544 (1990).
55. H. Ito, Y. Fukuda, K. Murata, A. Kimura, *ibid.* riol. **153**, 163 (1983).
56. R. R. Yocum, S. Hanley, R. W. West, M. Ptashne, *Mol. Cell. Biol.* **4**, 1985 (1984).
57. B. Gametchu and R. W. Harrison, *Endocrinology* **114**, 274 (1984).
58. J. Woolford, Jr., and M. Rotenberg, *Mol. Cell. Biol.* **6**, 674 (1986).
59. C. D. Clark-Adams, D. Norris, M. A. Osley, J. S. Fassler, F. Winston, *Genes. Dev.* **2**, 150 (1988).
60. J.-S. Lai and W. Herr, *Proc. Natl. Acad. Sci. U.S.A.* **89**, 6958 (1992).
61. We thank J. Tamkun, W. Kruger, and D. Moazed for communication of results prior to publication; M. Carlson, E. T. Young, and Roussel UCLAF for materials; J. M. Bishop, R. Grosschedl, A. Johnson, T. Parslow, J. Tamkun, and B. Yashinaga for critique of the manuscript; and A. Cordano for help with its preparation. Supported by grants from the NIH and postdoctoral fellowships from the NIH (S.K.Y.) and the Helen Hay Whitney Foundation (C.L.P.).

11 September 1992; accepted 30 October 1992

Phthalate Dioxygenase Reductase: A Modular Structure for Electron Transfer from Pyridine Nucleotides to [2Fe-2S]

Carl C. Correll,* Christopher J. Batie,† David P. Ballou, Martha L. Ludwig

Phthalate dioxygenase reductase (PDR) is a prototypical iron-sulfur flavoprotein (36 kilodaltons) that utilizes flavin mononucleotide (FMN) to mediate electron transfer from the two-electron donor, reduced nicotinamide adenine nucleotide (NADH), to the one-electron acceptor, [2Fe-2S]. The crystal structure of oxidized PDR from *Pseudomonas cepacia* has been analyzed at 2.0 angstrom resolution resolution; reduced PDR and pyridine nucleotide complexes have been analyzed at 2.7 angstrom resolution. NADH, FMN, and the [2Fe-2S] cluster, bound to distinct domains, are brought together near a central cleft in the molecule, with only 4.9 angstroms separating the flavin 8-methyl and a cysteine sulfur ligated to iron. The domains that bind FMN and [2Fe-2S] are packed so that the flavin ring and the plane of the [2Fe-2S] core are approximately perpendicular. The [2Fe-2S] group is bound by four cysteines in a site resembling that in plant ferredoxins, but its redox potential (−174 millivolts at pH 7.0) is much higher than the potentials of plant ferredoxins. Structural and sequence similarities assign PDR to a distinct family of flavoprotein reductases, all related to ferredoxin NADP$^+$-reductase.

A change in the currency of reducing equivalents, in which a flavin prosthetic group accepts two electrons as hydride ion (H^-) and donates one electron at a time to iron-sulfur centers or to cytochromes, is essential in the reaction pathways of respiration, photosynthesis, and biodegradation. To simplify crystallization and x-ray analysis of a protein catalyzing this conversion, we chose a bacterial oxidoreductase that is a natural fusion of flavoprotein and [2Fe-2S] domains. Phthalate dioxygenase reductase (PDR) is a component of the electron transfer chain involved in pyridine nucleotide–dependent dihydroxylation of phthalate in *Pseudomonas cepacia* (*1*, *2*). Thus PDR should provide a model for the many [2Fe-2S] flavoproteins that catalyze the initial steps in electron transfer chains. The geometry for electron transfer between flavins and other one-electron acceptors, including [4Fe-4S], cytochrome b, and cytochrome c, has been established from previously determined structures (*3*–*5*), and the mechanism of two-electron reduction of flavins by pyridine nucleotides (*6*) has been correlated with structure analyses of glutathione reductase (*7*).

Oxygenase systems typically comprise reductase, electron carrier, and terminal oxygenase components. When grown on phthalate, *P. cepacia* expresses two proteins: phthalate dioxygenase (PDO), a tetramer of 48-kD chains, and PDR, a 36-kD monomeric species (*1*, *8*). In this and related oxygenase systems (*2*, *9*), oxygen binding and hydroxylation occur at a mononuclear Fe^{2+} site in the dioxygenase component (*2*). Electrons from nicotinamide adenine nucleotide (NADH) are conveyed to the site for phthalate hydroxylation via three centers: flavin mononucleotide (FMN) and [2Fe-2S] in PDR and a Rieske [2Fe-2S] center (*10*) in PDO (*1*, *2*). The [2Fe-2S] center of PDR is presumed to be the site for electron transfer to PDO, since NADH-dependent substrate hydroxylation requires an intact [2Fe-2S] species to transfer electrons to the oxygenase component in related systems (*2*, *9*, *11*). Phthalate hydroxylation is catalyzed at a rate of at least 90 min^{-1} at 4°C (*12*) in the presence of both PDR and PDO; electron donors other than PDR do not support efficient oxygenation (*1*, *2*).

Redox equilibria favor electron transfer in the physiological direction: NADH → FMN → [2Fe-2S] → dioxygenase. The one-electron midpoint potentials at pH 7.0, determined by titration with dithionite, are −174 mV for the $FMNH^{\cdot}$-FMN couple, −284 mV for the $FMNH^-$-$FMNH^{\cdot}$ couple, −174 mV for the [2Fe-2S] cluster of PDR, and approximately −120 mV for the Rieske center in PDO (*12*). The potential of the [2Fe-2S] cluster of PDR, which is much higher than the potentials of −325 to −460 mV for plant ferredoxins (*9*), allows substantial population of the reduced [2Fe-2S] species during turnover.

Conversion of H^- to one-electron equivalents occurs in the reductive half-reaction of NADH with PDR (Fig. 1); the reaction has been studied by stopped-flow techniques. The internal electron transfer, which distributes one electron from fully reduced FMN to the [2Fe-2S] cluster of PDR (step 3), is rapid. A lower limit of 200 s^{-1} for the electron transfer rate has been derived from simulations with the stopped-flow data (*2*). The actual rate constant is likely to be much larger, since the structure now reveals that the FMN and a cysteine sulfur ligated to an iron are separated by an edge-edge distance of only 1.5 Å. Electron transfer in the analogous complex of ferredoxin with ferredoxin-NADP$^+$ reductase (FNR) occurs at 1500 to 7000 s^{-1} (*13*). The three rate-determining steps in the

The authors are in the Department of Biological Chemistry and Biophysics Research Division, University of Michigan, Ann Arbor, MI 48109.

*Present address: Department of Molecular Biophysics and Biochemistry, Yale University, New Haven, CT 06511.
†Present address: Department of Biochemistry, Louisiana State University Medical Center, New Orleans, LA 70112.

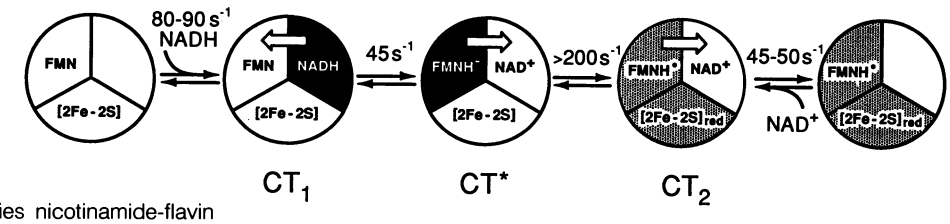

Fig. 1. Reduction of PDR by NADH. Intermediates in the two-electron reduction of PDR at 4°C, pH 8.0, 0.1 M Hepes, are shown schematically (*1, 2, 12*). The black, gray, and white wedges represent two-electron reduced, one-electron reduced, and oxidized species, respectively, and the arrows represent charge-transfer species, with the arrow pointing toward the acceptor. Charge-transfer absorbance signifies nicotinamide-flavin stacking in the transient intermediates (*49*). The spectrascopic characteristics of CT_1 are consistent with charge transfer between the reduced nicotinamide ring and oxidized flavin. Hydride transfer in step 2, which displays an isotope effect with NADD as substrate (*1*), reduces the flavin to the hydroquinone form, but the expected charge-transfer species with flavin hydroquinone as donor and oxidized pyridine ring as acceptor, CT*, is not observed; therefore the rate constant for the decay of CT* (one-electron transfer to [2Fe-2S]) is much larger than the rate constant for its formation. CT_2 is a charge-transfer complex between flavin semiquinone and oxidized nicotinamide, in which the [2Fe-2S] center is reduced; CT_2 can also be generated by addition of NAD^+ to PDR^{2-} (*12*).

reductive half-reaction are formation of an initial charge-transfer complex between NADH and PDR (CT_1), hydride transfer, and release of NAD^+. The structures of PDR complexed with pyridine nucleotides, reported here, suggest that structural rearrangements may affect the rates of CT_1 formation and product release.

Structure determination and description. The structure was determined by means of multiple isomorphous replacement supplemented with phase information from partial models (*14*). The initial phases came from two heavy atom derivatives, lead acetate (two sites) and osmium hexachloride (two sites). The tightly bound ADP (adenosine diphosphate) moiety of NAD^+ produced intensity changes large enough for the NAD^+ complex to serve as a third derivative in subsequent phasing, and native anomalous scattering differences were incorporated by suitably weighted phase combination (*15*) (Tables 1 and 2). Refinement was begun with coordinates that were the result of five cycles of model building and phase combination. The amino acid sequence (Fig. 2) was derived from the sequences of proteolytic fragments and from the x-ray structure (*8*).

The binding determinants for the pyridine nucleotide substrate and for each of the prosthetic groups, FMN and [2Fe-2S], are found primarily in the individual domains (Fig. 3). The three domains are arranged along the primary sequence from the amino- to the COOH-terminus in the order FMN domain (residues 1 to 102), NAD domain (residues 112 to 226), and [2Fe-2S] domain (residues 236 to 321), and their simple connection suggests evolution by fusion at the DNA level. Domain-domain packing places the isoalloxazine group of FMN at a central cleft in the molecule, where it is optimally positioned to mediate the overall electron transfer from NADH to [2Fe-2S]. The NH_2-terminal FMN domain is a six-stranded antiparallel β barrel with the Greek key topology 1, 3, −1, −1, 3. This particular topology occurs in pyruvate kinase (*16*), but it is a newly recognized motif for binding flavins, found thus far only in PDR and FNR (*17*). The NAD domain is an α/β fold (*18*), and the [2Fe-2S] domain, a five-stranded mixed β sheet with connections −1, 3x, 1, −2x, has the same topology as the plant-type ferredoxins (*19, 20*).

The orientation of FMN is controlled by its interactions with the NH_2-terminal domain. Hydrogen bonding to the pyrimidine portion of the flavin positions the isoalloxazine ring with its *si* side facing inward toward the FMN domain (Fig. 4). The FMN phosphate is anchored to the start of helix Fα1 by interactions with peptide amides and with a serine and two arginine residues, and the sequence 55 to 58 provides contacts to N(5) and the *si* face (Fig. 4) of the flavin ring. As a result of these intradomain interactions, the *re* side of the isoalloxazine ring is presented to the NAD domain and the dimethylbenzene end protrudes toward the [2Fe-2S] domain. In flavoprotein electron transferases such as flavodoxins (*21*) and FNR (*17*), the dimethylbenzene moiety is accessible for solvent or intermolecular contact and appears to be utilized for electron transfer.

As in plant ferredoxins, the [2Fe-2S] cluster in PDR is bound at the periphery of its domain by four cysteine ligands. The three cysteine residues at 272, 277, and 280 are part of a loop that closely resembles the $CyS\text{-}X_4\text{-}CyS\text{-}X_2\text{-}CyS$ binding sites of [2Fe-2S] ferredoxins (*9, 19*). Despite the many structural similarities between the plant ferredoxins and the [2Fe-2S] domain of PDR, the redox potential of [2Fe-2S] in PDR is higher by approximately 250 mV. Comparison with ferredoxin from *Anabaena 7120* reveals two clear differences in local protein:[22Fe-2S] interactions. Thr^{276}, which hydrogen bonds to Sγ 272 in PDR, is replaced by Ala in *Anabaena* Fd. In addition, the orientation of the peptide dipole at 277 to 278 is opposite in the two proteins, with the negative carbonyl oxygen of Cys^{277} away from the cluster in PDR, instead of toward it, as in Fd. Substantial

Table 1. Data collection and structure determination. Crystals of oxidized PDR (space group *R*3, $a = b = 114.4$, $c = 77.9$ Å) were grown from seeds in hanging drops in PEG-6000, 50 mM MES, pH 6.7, at 4°C (*25*). Intensities were measured at 4°C (Xuong-Hamlin dual area detector). Preliminary soaking times for preparation of the $Pb(Ac)_2$ and K_2OsCl_6 derivatives were 4 and 24 hours, respectively. Heavy-atom parameters were refined with HEAVY (*43*) and then PHARE (*44*). Parameters for the two native irons were refined with MADSYS (*45*). Initial models were fit to maps calculated with data to 2.9 Å having phases based on $Pb(Ac)_2$ and K_2OsCl_6 derivatives, the NAD^+ complex, and anomalous scattering differences from the native protein ($\langle m \rangle = 0.62$). Density corresponding to the FMN was evident in these maps. Model building was assisted by selecting conformations from the structure database in the TOM (*46*) package. The coordinates of spinach ferredoxin-$NADP^+$-reductase (*17*) and of ferredoxin from *Anabaena 7120* (*19*) were made available for comparison at a stage when the partial model ($R = 0.493$) included 269 residues.

Parameter	Native*	Native anomalous†	$Pb(Ac)_2$ (2 mM)‡	K_2OsCl_6 (1 mM)	NAD^+:PDR (10 mM)	NADH:PDR^{2-} (10 mM)§
Resolution (d_{min}, Å)	2.0	2.3	2.7	3.1	2.7	2.7
Unique reflections (no.)	23,943	15,799	9,402	5,249	9,379	8,874
Completed (%)	93	94	90	76	90	89
Fold redundancy at d_{min}	3.9	2.7	2.8	2.3	1.7	1.8
$I/\sigma(I)$ at d_{min}	2.1	2.9	2.4	3.5	3.6	3.2
R_{sym}	6.2	4.8	4.8	2.8	4.1	3.8
$\langle F_h \rangle$rms/EII			2.1	4.9	1.7	

*This data set was used in the final refinement (Table 2). †Bijvoet pairs were measured by means of the inverse beam method. Data from three crystals were merged. ‡Because of rapid decay, four crystals were required; the data were merged. §Reduction and mounting were carried out in an anaerobic glove box. IIEr, closure error.

Fig. 2. The primary and secondary structures of PDR. The underlined regions of the PDR sequence were determined by sequence analysis of the intact protein or of peptide fragments; the remaining residues were identified from electron density maps. [The sequence of the structural gene verifies the identification of residues interacting with substrate and prosthetic groups (*8*).] Peptides were generated by digestion with trypsin, lysC, or clostripain and sequenced by standard protocols (*50, 51*). The homology between PDR and the functionally related protein, vanillate demethylase oxidoreductase (VanB) (*52*), simplified the placement of sequenced fragments and assisted the residue assignments from electron densities. The secondary structures (α and β) were assigned as described (*34, 41*). The domains are designated as follows: F, FMN; N, NAD; and I, [2Fe-2S]. As each fragment was incorporated into the atomic model, agreement with the x-ray data was confirmed by computation of weighted difference maps calculated by the program SIGMAA (*14*), with phases obtained from simulated annealing refinement of the partial model. The procedure resembled that used in two other structure determinations (*53*). Both the NH_2- and COOH-termini are visible in the maps, but the main chain is disordered at residues 228 to 234 and residues 297 to 302. These disordered residues were assigned as alanines where chemical sequences were undetermined. Abbreviations for the amino acid residues are: A, Ala; C, Cys; D, Asp; E, Glu; F, Phe; G, Gly; H, His; I, Ile; K, Lys; L, Leu; M, Met; N, Asn; P, Pro; Q, Gln; R, Arg; S, Ser; T, Thr; V, Val; W, Trp; and Y, Tyr.

```
         10         20         30         40         50         60
TTPQEDGFLRLKIASKEKIARNIWSFELTNPQGAPLPPFEAGANLTVAVPNGSRRTYSLC
         |<--Fβ1--->|  |<Fβ2>|              |<Fβ3>|    |<Fβ4|

         70         80         90        100        110        120
NESSERDRYTIAVKRDSNGRGGSISFIDDTSEGDAVEVSLPRNEFPLDKRAKSFILVAGG
         |<Fβ5>|      |<-Fα1->|    |<-Fβ6->|           |<-Nβ1>|

        130        140        150        160        170        180
IGITPMLSMARQLRAEGLRSFRLYYLTRDPEGTAFFDELTSDEWQSDVKIHHDHGDPTKA
  |<---Nα1---->|    |<Nβ2->|        |<Nα2|      |<Nβ3>|

        190        200        210        220        230        240
FDFWSVFEKSKPAQHVYCCGPQALMDTVRDMTGHWPSGTVHFESFGGAAAAAAANTADTV
  |Nα3|      |<Nβ4>|  |<-Nα4-->|        |Nβ5|              |Iβ1

        250        260        270        280        290        300
RDARSGTSFEIPANRSINQVLRDANVRVPSSCESGTCGSCKTGLCSGAADHRDDVLAAAA
->|   |<Iβ2>|  |<-Iα1->|                | Iβ3-Iβ3'|

        310        320
KGTQIMVCVSRAKSAELVLDL
  |Iβ4|  |Iβ5-Iβ5'|
```

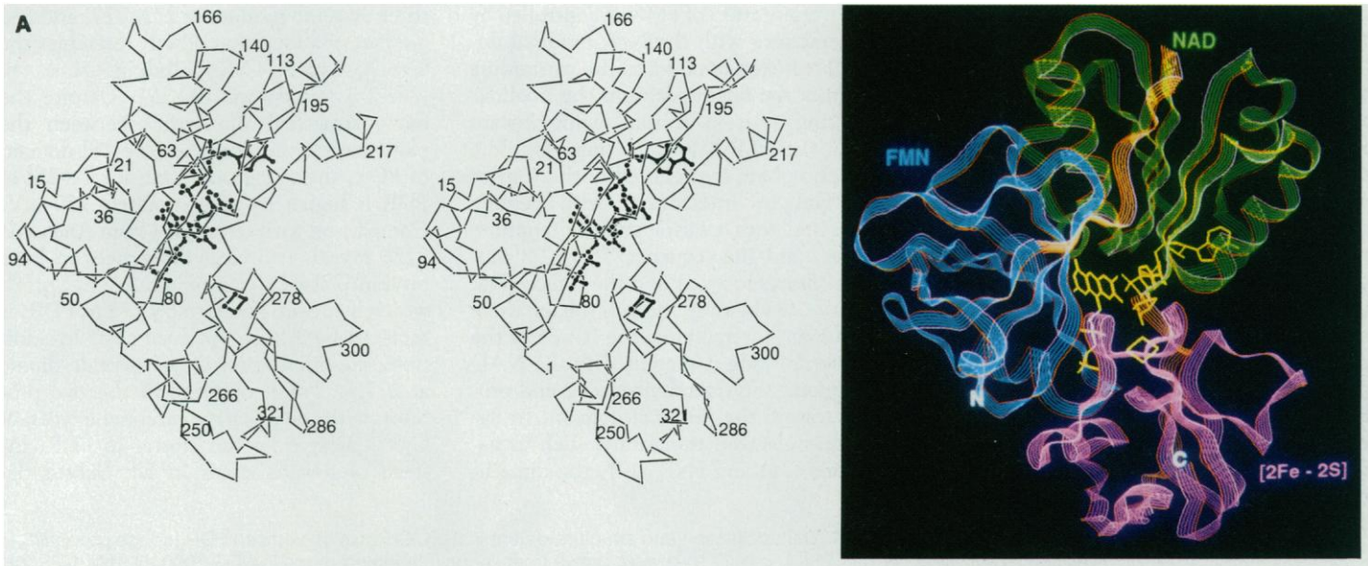

Fig. 3. The conformation of PDR. (**A**) A stereoview of the Cα backbone of PDR. All atoms of the FMN, [2Fe-2S], and bound pyridine nucleotide groups are represented to show the arrangement of the three redox components; this perspective presents the *si* face of the flavin ring to the viewer. The cleft between the FMN and [2Fe-2S] domains is a likely site binding PDO. (**B**) A ribbon representation of PDR that distinguishes the three domains and indicates the secondary structures in each domain. The domain connectors are shown in gold. The viewpoint is rotated slightly from (A) to display the domain divisions and connectors more clearly. (**C**) Sheet topologies for each of the domains, with nomenclature as in Fig. 2. The β strands are represented by arrows and the helices are represented as cylinders, with front helices having thickened outlines. In the first domain, FMN hydrogen bonds to the Fβ4 and Fβ5 strands to close the barrel. The nucleotide binding domain has the connecting topology −1×, −1×, 3×, 1× and does not have the sixth strand found in lactate dehydrogenase (*18*).

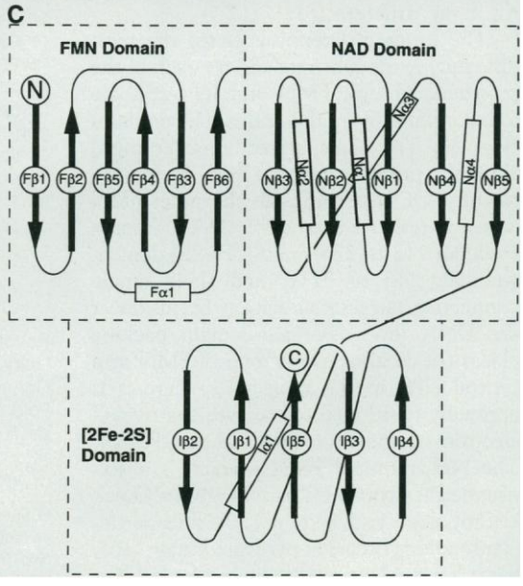

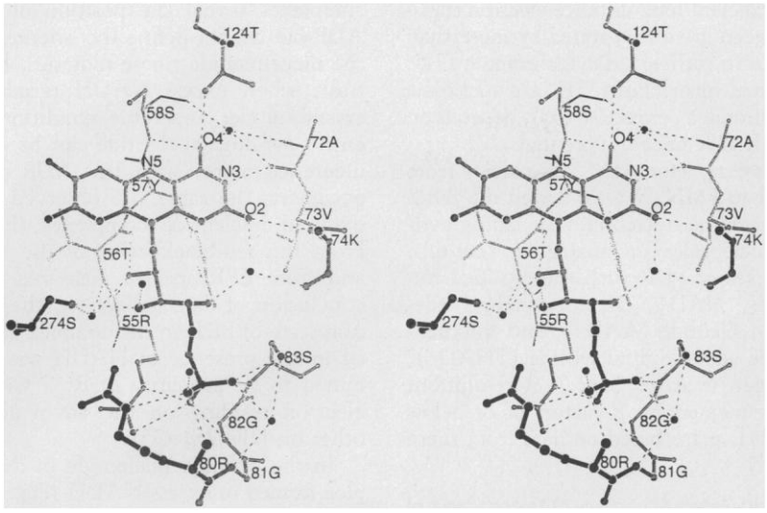

Fig. 4. The FMN binding site in PDR. A stereoview with hydrogen bonds represented as dashed lines and solvents drawn as filled circles. The view is toward the *re* face of the flavin from outside the FMN domain, with the pyrimidine end of the isoalloxazine to the right. Isoalloxazine heteroatoms N(5), O(4), N(3), and O(2) form hydrogen bonds [contacts <3.4 Å with acceptable angles (*54*)] to Ser^{58}, Ala^{72}, and Lys^{74}, and the ribityl O(3)* interacts with Ser^{274}.

variations in residues surrounding the [2Fe-2S] cluster are also expected to affect the potentials (*22*).

Geometry for one-electron transfer between FMN and [2Fe-2S]. The iron-sulfur binding loop, S^{271}C-E-S-G-T-C-G-S-C, plays a key role in the FMN:[2Fe-2S] interface, packing against FMN and the Fβ4 strand of the barrel motif that binds FMN. Direct and water-mediated hydrogen bonds, as well as van der Waals contacts, hold the domains together (Fig. 5B). The domain packing orients the prosthetic groups so that the planes of the [2Fe-2S] core and isoalloxazine atoms are nearly perpendicular, with the Fe-Fe vector virtually parallel to the plane of the flavin ring (Fig. 5B). Although the Fe atoms of the iron-sulfur cluster are insulated from solvent or interdomain contacts, Fe1, the atom closer to the surface of the domain, is only 7.2 Å from the flavin 8-CH_3. Recent ^{1}H NMR (nuclear magnetic resonance) studies (*23*) indicate that the reducible iron (*24*) in plant ferredoxins is the iron analogous to Fe1 of PDR. The disparity in hydrogen bonding to the Fe1 and Fe2 ligands in PDR (Fig. 5) also suggests that Fe1 of PDR is reduced by electron transfer from the flavin.

The relative positions and separations of the FMN and [2Fe-2S] groups in PDR are similar to those observed for FMN and [4Fe-4S] in trimethylamine dehydrogenase (*4*), where the flavin 8-CH_3 is also the atom nearest to the iron-sulfur center. However, the close juxtaposition of chromophores in PDR was not initially predicted from the EPR (electron paramagnetic resonance) spectrum of PDR^{2-} (*2*, *25*), which displays *g* values close to those typical for isolated flavin semiquinone (g = 2.0) and reduced [2Fe-2S] clusters of plant ferredoxins (g = 2.05, 1.94, and 1.89). Interaction between the reduced [2Fe-2S] center and the FMN radical is in fact evident in EPR spectra of frozen solutions. The spectrum appears at first glance to be a sum of semiquinone and reduced [2Fe-2S] signals. Although the spectrum integrates to two electrons, the apparent semiquinons signal at g = 2.0 accounts for only 15 percent of the total spin (*26*).

Edge-edge distances and electronic coupling between donor and acceptor are crucial parameters determining the rates of biological electron transfer reactions (*27*). Delocalization of electrons from reduced [2Fe-2S] to the β-CH_2 and α-CH of cysteine, and to backbone nitrogen atoms, is deduced from NMR spectra of plant ferredoxins (*24*). ENDOR measurements indicate significant spin density on the 8-CH_3 of flavin semiquinones in the electron

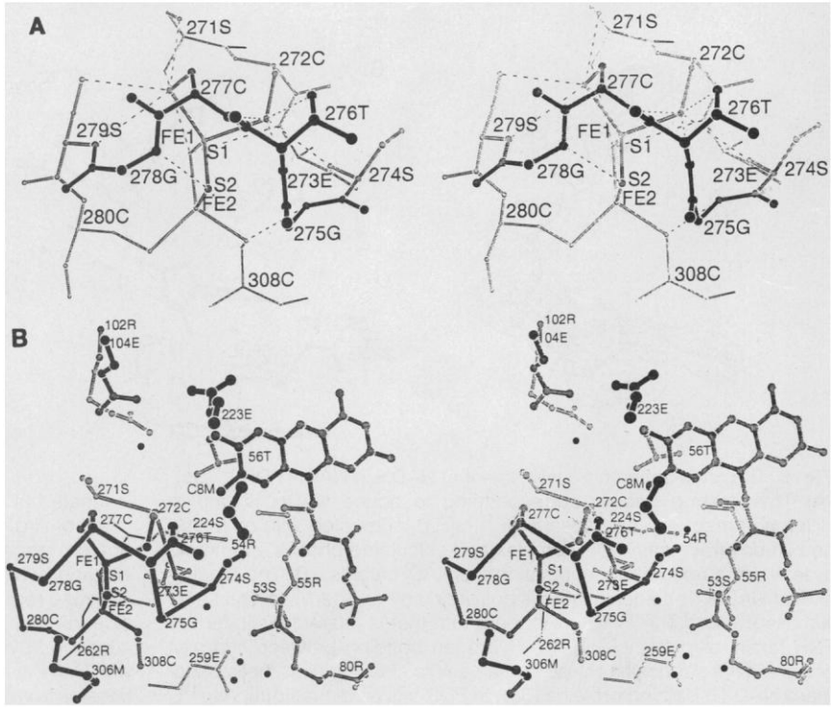

Fig. 5. The [2Fe-2S] prosthetic group and its environment in PDR. (**A**) The [2Fe-2S] cluster and its intradomain interactions. The backbone torsion angles of loop residues 271 to 280 are like those in plant ferredoxins (*19*), except at 277 to 278 (see text). Predominant among the cluster contacts are NH-Sγ hydrogen bonds and hydroxyl side chain–Sγ hydrogen bonds [contacts <3.5 Å and acceptable angles (*54*)] and the nonpolar interaction with CH_3 of Met^{306} (B), which adjoins S2 of the [2Fe-2S] cluster. (**B**) The interface for electron transfer. Residues from the FMN domain are to the right and upper left; residues 223 and 224, toward the viewer, are from the NAD domain. To emphasize the fold around the [2Fe-2S] cluster, bonds are drawn connecting the Cα of residues 271 to 280. The approach of the 8-CH_3 of the FMN ring to the β-CH_2 of Cys^{272} can be seen near the center of the drawing. Interdomain hydrogen bonds connect Thr^1 (not shown), Ser^{53}, Thr^{56}, Arg^{80}, and ribityl O(3)* with Arg^{262}, Asn^{265}, Glu^{259}, Cys^{272}, Glu^{273}, and Ser^{274}. Six solvents (filled circles) bridge protein groups from the FMN and [2Fe-2S] domains. Charged residues in the interface include Glu^{223}, near the flavin 7-CH_3, and Glu^{102}, hydrogen-bonded to Arg^{104}.

transferase, flavodoxin (28). Thus, the observed orientation of the chromophores in PDR results in close approach of the orbitals that take part in electron transfer. From the positions of the $Cys^{272}S$ ligand of Fe1 and the flavin 8-CH_3, we calculate a van der Waals edge-edge separation of only 1.5 Å. This very short donor-acceptor distance (Fig. 5B) is like some of the short transfer distances in the photoreaction center (29) and is similar to interaction distances postulated for reactions between electron transfer proteins such as flavodoxin and cytochrome c (30). The close approach of donor and acceptor in PDR may be important for rapid distribution of electrons when the potentials of the centers are nearly equal. Efficient long-distance electron transfer between groups separated by more than 10 Å, as in ruthenated cytochrome c (31), ruthenated myoglobin (32), or cytochrome c:cytochrome c peroxidase (33), depends on a suitable difference in potential (27).

Geometry for H^- transfer from NADH to FMN. We examined the binding of pyridine nucleotides by adding pyridine nucleotides or analogs to crystals. Complexes of PDR with the oxidized nucleotides, NAD^+, 3-aminopyridine adenine dinucleotide (AAD^+), and thionicotinamide adenine dinucleotide ($TNAD^+$), have been analyzed at 2.7 Å resolution. After refinement to *R* factors at or below 0.20 (34), maps based on data from these complexes reveal the position of bound ADP but do not define the orientation of the nicotinamide ribose moieties. In contrast, when excess NADH is added to crystals under anaerobic conditions, the entire pyridine nucleotide can be seen in difference maps, with the ADP portion occupying the same site observed in the oxidized nucleotide complexes (Fig. 6). From the red-black color of the crystals and from EPR spectra measured at the conclusion of data collection, the oxidation state of PDR in the complex generated in the presence of NADH was determined to be primarily PDR^{2-}, with one electron residing on the flavin and the other on [2Fe-2S] (35).

In the pyridine nucleotide in the complex formed in excess NADH (Fig. 6), the nicotinamide binds near the COOH-terminal ends of strands Nβ1 and Nβ4 of the parallel β sheet of the NAD domain. The adenine ring is positioned between a loop formed by residues 173 to 179 and Nα4, and the pyrophosphate is adjacent to the NH_2-terminus of Nα1. The pyrophosphate binding sequence is distinctive in PDR and in the FNR family (Fig. 7). Small but significant structural changes are induced in the vicinity of the ADP portion of the bound pyridine nucleo-tide. Residues 173 to 179 adjust to allow Asp^{173} to hydrogen bond to both alcohol groups of the adenosine ribose (Fig. 6B), and the guanidinium group of Arg^{148} moves about 4 Å to interact with the AMP phosphate.

Stacking or contact between the nicotinamide group and the flavin ring is expected in hydride transfer reactions (6) (Fig. 1).

Table 2. Refinement of PDR by XPLOR. Each round of simulated annealing (SA) consisted of dynamics runs at high temperature followed by either slow (47) or fast cooling. In stage I, starting temperatures of 3000° and 4000°C were used; for stages II and III, the temperatures were decreased to 1000° or 2000°C. The stereochemistry was optimized by means of Powell minimization for 120 cycles before and after the heating stage; B factors were refined at the end of each cycle. Confirmed peptide sequences were incorporated before the initial refinement. Refinements in stages I and II were made from the data set with Friedel pairs measured explicitly (Table 1); the first round included only data between 5.0 and 2.0 Å. The concluding refinements (stage III) used the 2.0 Å data set (Table 1). Solvent molecules were added only if they were associated with one of the 225 chemically confirmed residues. For the model reported here, the root mean square bond length deviation was 0.015 Å, and the bond angle deviation was 3.1°. The mean coordinate error range of 0.20 to 0.26 Å from the Luzatti plot (48) was in good agreement with the 0.23 Å determined from the sigma A plot (14). Three residues, Ala^{234}, Asn^{235}, and Arg^{311}, fell outside of the energetically preferred regions on a Ramachandran plot.

Stage	Rounds of simulated annealing	Resolution (Å)	Reflections (no.)	R_{start}	R_{end}	Atoms (water) in last cycle (no.)
I	1 to 3	10.0 to 2.7	9,994	0.420	0.233	2292 (0)
II	4 to 6	10.0 to 2.3	15,599	0.307	0.227	2379 (0)
III	7 to 17	40.0 to 2.0	21,912	0.269	0.202	2597 (118)

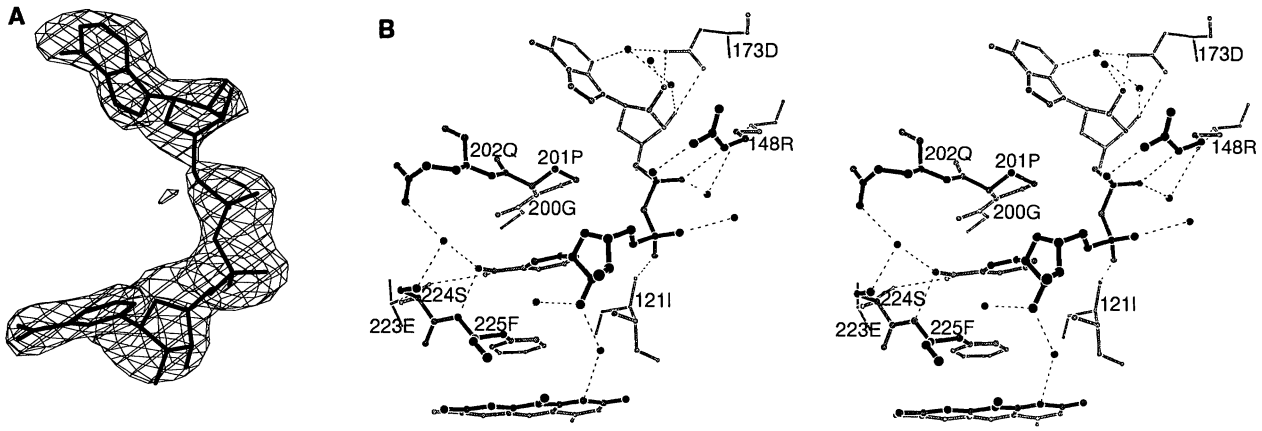

Fig. 6. The orientation and environment of NADH in NADH:PDR^{2-} (35). (**A**) The electron density corresponding to bound NADH is from a difference map with coefficients ($|F_o| - |F_c|$), computed with observed amplitudes from the NADH complex and calculated phases and amplitudes from a refined model omitting the NADH atoms. (**B**) The binding site for NADH. The adenine ring is positioned by van der Waals contacts with Asp^{173} and Thr^{207}. I^{121} is in the β turn that is characteristic for the FNR family of proteins (Fig. 7). Hydrogen bonding between hydroxyl groups in the adenosine ribose and an acidic side chain is a hallmark of many NAD(H) binding proteins (38); in PDR this acidic residue, Asp^{173}, is located at the COOH-terminal end of β3 (17). Asp^{173} and the side chain of Arg^{148} have moved to interact with the ribose and phosphate groups, respectively. The ring of Phe^{225} is in the "gate-closed" position, stacked between the flavin and the nicotinamide group. As shown, the structure requires the nicotinamide moiety to approach FMN from the *re* side of the isoalloxazine ring; in FNR, *re* side transfer has been confirmed by ^2H labeling experiments (6). Reduction of PDR by NADD with D in the pro-R position yields unlabeled NAD^+, establishing A-side transfer from the pyridine nucleotide (1).

In the structure of NADPH bound to reduced glutathione reductase (*7*), a Tyr residue is displaced by the nicotinamide moiety to form a complex in which the nicotinamide stacks against the flavin ring. However, in the NADH:PDR^{2-} complex (*35*), the nicotinamide ring is not oriented as expected for hydride transfer (Fig. 6). Instead it is sandwiched between Pro^{201} and Phe^{225} in a pocket formed by the pyrophosphate binding sequence, the helical turn at the start of Nα4, and the ring of Phe^{225}. The observed binding is presumed to represent an alternative mode of interaction between reduced pyridine nucleotide and reduced enzyme. Model building and comparison with known conformations of pyridine nucleotides suggest that Phe^{225} can be displaced to permit nicotinamide-flavin stacking. In the model complex the ADP moiety occupies the same binding subsite observed. The structural changes necessary to stack the nicotinamide over the flavin ring are akin to the opening or closing of a gate and require some displacement of the protein backbone as well as movement of the side chain of Phe^{225}. These rearrangements may limit the rates of CT_1 formation and product release (Fig. 1), both of which contribute to the observed rate of reduction (*2*).

Analysis of NADH:PDR^{2-} and of the fully reduced species (PDR^{3-}) at 2.7 Å (*34*) reveals additional structural changes that accompany reduction. Two rearrangements that stabilize the reduced species are observed in the vicinity of the flavin ring in the semiquinone and fully reduced hydroquinone forms: the Oγ of Ser^{58} moves closer to N(5) to form a hydrogen bond and a solvent moves to interact with N(1) of the flavin. Difference maps and refinement indicate small shifts of the [2Fe-2S] domain and local changes in the iron-sulfur loop and [2Fe-2S] cluster.

PDR and the FNR family of proteins. The structures of FNR and PDR have equivalent folding topologies; fitting the backbone atoms superimposes the structures with a root-mean-square positional discrepancy of 1.9 Å for 176 equivalent residues. The core secondary structures of the FMN and NAD domains align well, while most of the additional residues that are present in FNR are folded into surface loops. Thus a sequence alignment of FNR with PDR can be derived from the spatial equivalences of residues in the FMN and NAD domains even though there is less than 20 percent identity of the core residues. The combined three-dimensional and sequence alignments of PDR with FNR identify PDR as a member of the family of protein folds characterized by Karplus *et al.* (*17*). The family currently includes cytochrome P-450 reductase, cytochrome b_5 reductase, sulfite reductase, nitrate reductase, the COOH-terminal portion of nitric oxide synthase, and methane monooxygenase reductase (*17, 36, 37*).

Members of the extended FNR family all share flavin and pyridine nucleotide binding sequences arranged in the order flavin → pyridine nucleotide. Several chemical features appear to be conserved: the hydroxyl groups at positions 58 and 83 (PDR numbering), important for flavin reduction and phosphate binding, respectively; the aromatic residue acting as a gate in nicotinamide binding; and the type II′ XGXG turn, which defines the FNR variant (*17*) of the common nucleotide phosphate loop (*18, 38*). All members of the family are associated with a third component, an electron carrier located on a separate polypeptide chain (*39*) or linked to the FNR domains. Among the fusion proteins identified as members of the FNR family, many have incorporated the electron carrier domain at the NH_2-terminus; but in two, including PDR, the carrier sequences are fused to the COOH-terminus of FNR-like domains. The ability to swap positions of the carrier domain in the fusion proteins verifies that the third domain is an independent modular unit. The structure of PDR suggests that either order could be accommodated without altering the orientation of the [2Fe-2S] domain; the Cα of the NH_2- and COOH-termini of PDR can easily be connected by a short linker as illustrated in Fig. 7B.

If the sequences that fingerprint flavin and pyridine nucleotide binding are a valid guide, we may assume that the flavin and pyridine nucleotide binding domains will be similar for all the proteins in the families defined in (*17*) and in (*36, 37*), with the 7-CH_3 and 8-CH_3 groups of the flavin exposed for electron transfer. Interaction with the one-electron donor-acceptor domain is predicted to occur in the same region where the [2Fe-2S] domain interface is located in PDR. Hence the structure of PDR not only affords a model for studies of electron transfer per se but also suggests a mode of assembly of domains in the extended FNR family.

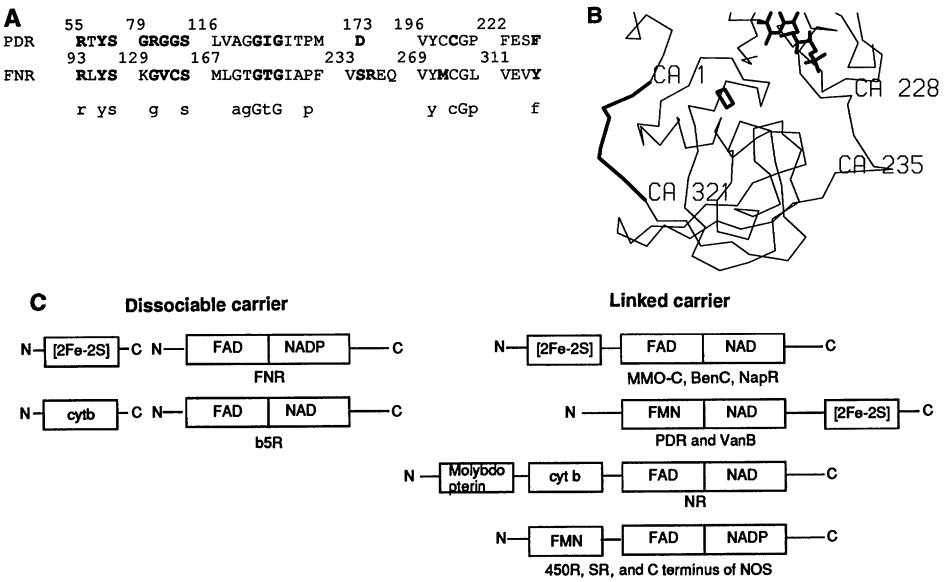

Fig. 7. Conserved sequences in the FNR family. (**A**) Six peptide segments involved in recognition of flavin nucleotides and pyridine nucleotides provide a fingerprint for the extended FNR family of proteins (*17, 36, 37*). The alignment of FNR (*55*) with PDR is based on superpositions of the two structures; residues that interact with substrate or prosthetic groups are bold. The consensus fingerprint sequence, shown in the third line, is that proposed by Andrews *et al.* (*36*), with invariant residues in uppercase and conserved residues in lowercase letters. (**B**) A drawing of the alternative fusions of the [2Fe-2S] domain to the FNR module. The linker actually found in PDR occurs at 228 to 235; a linker that could fuse the [2Fe-2S] domain to the NH_2-terminus of the FMN domain is drawn connecting 321 to 1 (*34*). (**C**) The domain arrangements of selected members of the flavoprotein electron transferase family (*17, 36, 37*). Abbreviations are: b5R, cytochrome b_5 reductase; MMO-C, methane monooxygenase component C; BenC, benzoate 1,2-dioxygenase reductase; NapR, NADH-ferredoxin$_{NAP}$ reductase (*56*); VanB, vanillate demethylase oxidoreductase, presumed to bind FMN; SR, sulfite reductase α; 450R, cytochrome P450 reductase; NOS, nitric oxide synthase; and NR, nitrate reductase. Andrews *et al.* (*36*) have proposed that NOS, P450R, and SR incorporate insertions in their FAD domains.

REFERENCES AND NOTES

1. C. J. Batie, E. LaHaie, D. P. Ballou, *J. Biol. Chem.* **262**, 1510 (1987); C. J. Batie and D. P. Ballou, in *Flavins and Flavoproteins 1987*, D. E. Edmondson

and D. E. McCormick, Eds. (de Gruyter, Berlin, 1987), pp. 377–380.
2. C. J. Batie, D. P. Ballou, C. C. Correll, in *Chemistry and Biochemistry of Flavoenzymes*, F. Müller, Ed. (CRC Press, Boca Raton, FL 1992), vol. 3, pp. 543–556; D. B. Ballou and C. Batie, in *Oxidases and Related Redox Systems*, T. E. King, H. S. Mason, M. Morrison, Eds. (Liss, New York, 1988), pp. 211–226.
3. L. W. Lim *et al.*, *J. Biol. Chem.* **261**, 15140 (1986).
4. Z.-X. Xia and F. S. Mathews, *J. Mol. Biol.* **212**, 837 (1990).
5. F. S. Mathews, Z.-W. Chen, H. Bellamy, *Biochemistry* **27**, 238 (1991).
6. D. J. Manstein, V. Massey, E. F. Pai, in *Flavins and Flavoproteins 1987*, D. E. Edmondson and D. B. McCormick, Eds. (de Gruyter, Berlin, 1987), pp. 3–12; V. Massey and S. Ghisla, in *Biological Oxidations*, H. Sund and V. Ullrich, Eds. (Springer-Verlag, Berlin, 1983), pp. 114–139; C. Walsh, *Acc. Chem. Res.* **13**, 148 (1980).
7. P. A. Karplus and G. E. Schulz, *J. Mol. Biol.* **195**, 701 (1987); *ibid.* **210**, 163 (1989); E. F. Pai, P. A. Karplus, G. E. Schulz, *Biochemistry* **27**, 4465 (1988).
8. The DNA encoding PDR from *Pseudomonas cepacia* was cloned and sequenced by R. Liu and G. Zylstra [private communication; *Abstr. Annu. Meet. Am. Soc. Microbiol.* **1992**, 262 (1992)]. In Fig. 2, we do not report the protein sequence deduced by them, but the length of the linker between NAD and [2Fe-2S] domains has been adjusted to accord with the DNA sequence analysis.
9. R. Cammack *et al.*, *Biochem. J.* **168**, 205 (1977); R. Cammack, *Adv. Inorg. Chem.* **38**, 1 (1991).
10. Rieske iron-sulfur clusters are bound to proteins by two cysteine and two histidine ligands rather than by four cysteines (*40*).
11. J. Lund, M. P. Woodland, H. Dalton, *Eur. J. Biochem.* **147**, 297 (1985); M. Yamaguchi and H. Fujisawa, *J. Biol. Chem.* **256**, 6783 (1981).
12. C. J. Batie, L. Wang, G. Gassner, D. P. Ballou, in preparation; G. Gassner and D. P. Ballou, in preparation.
13. A. K. Bhattacharyya, T. E. Meyer, G. Tollin, *Biochemistry* **25**, 4655 (1986); M. C. Walker, J. J. Pueyo, C. Gomez-Moreno, G. Tollin, *Arch. Biochem. Biophys.* **281**, 76 (1990).
14. R. J. Read, *Acta Crystallogr. Sect. A* **42**, 140 (1986); *ibid.* **46**, 900 (1990).
15. W. A. Hendrickson and E. E. Lattman, *Acta Crystallogr. Sect. B* **26**, 136 (1970).
16. J. S. Richardson, *Adv. Protein Chem.* **34**, 167 (1981).
17. P. A. Karplus, M. J. Daniels, J. R. Herriott, *Science* **251**, 60 (1991).
18. M. G. Rossmann, D. Moras, K. W. Olsen, *Nature* **250**, 194 (1974).
19. W. R. Rypniewski *et al.*, *Biochemistry* **30**, 4126 (1991).
20. Although the fifth strand has not previously been described, the program DSSP (*41*) assigns equivalent secondary structures to *Anabaena* ferredoxin (Brookhaven Data Bank entry 1FXA).
21. M. L. Ludwig and C. L. Luschinsky, in *Chemistry and Biochemistry of Flavoenzymes*, F. Müller, Ed. (CRC Press, Boca Raton, FL, 1992), vol. 3, pp. 427–466; S. G. Mayhew and G. Tollin, *ibid.*, pp. 389–426.
22. G. Backes *et al.*, *J. Am. Chem. Soc.* **113**, 2055 (1991).
23. L. B. Dugad, G. N. La Mar, L. Banci, I. Bertini, *Biochemistry* **29**, 2263 (1990).
24. W. R. Dunham, G. Palmer, R. H. Sands, A. J. Bearden, *Biochim. Biophys. Acta* **253**, 373 (1971); M. Poe, W. D. Phillips, C. C. McDonald, W. Lovenberg, *Proc. Nat. Acad. Sci. U.S.A.* **65**, 797 (1970); I. Salmeen and G. Palmer, *Arch. Biochem. Biophys.* **150**, 767 (1972); L. Skjeldal *et al.*, *Biochemistry* **30**, 7363 (1991).
25. C. C. Correll, C. J. Batie, D. P. Ballou, M. L. Ludwig, *J. Biol. Chem.* **260**, 14633 (1985).
26. EPR measurements were conducted by W. R. Dunham. The spin-spin interactions were different from those seen when substrate was added to the [4Fe-4S] protein trimethylamine dehydrogenase (TMADH); the EPR spectrum of TMADH reduced by substrate shows little resemblance to the spectra of the isolated components (*3*).
27. R. A Marcus and N. Sutin, *Biochim. Biophys. Acta* **811**, 265 (1985); H. B. Gray and B. G. Malmström, *Biochemistry* **28**, 7499 (1989); C. C. Moser, J. M. Keske, K. Warnke, R. S. Farid, P. L. Dutton, *Nature* **355**, 796 (1992); *Electron Transfer in Biology and the Solid State*, M. K. Johnson *et al.*, Eds. (Advancs in Chemistry Series, 226, American Chemical Society, Washington, DC, 1990).
28. J. Fritz, F. Müller, S. G. Mayhew, *Helv. Chim. Acta* **56**, 2250 (1973).
29. J. Deisenhofer and H. Michel, *EMBO J.* **8**, 2149 (1989).
30. G. Tollin, T. E. Meyer, M. A. Cusanovich, *Biochim. Biophys. Acta* **853**, 29 (1986).
31. A. W. Axup, M. Albin, S. L. Mayo, R. J. Crutchley, H. B. Gray, *J. Am. Chem. Soc.* **110**, 435 (1988); J. A. Cowan, R. K. Upmacis, D. N. Beratan, J. N. Onuchie, H. B. Gray, *Ann. N.Y. Acad. Sci.* **550**, 68 (1988).
32. T. J. Meade, H. B. Gray, J. R. Winkler, *J. Am. Chem. Soc.* **111**, 4353 (1989).
33. G. McLendon, *Acc. Chem. Res.* **21**, 160 (1988); S. Hahm, B. Durham, F. Millet, *Biochemistry* **31**, 3472 (1992).
34. C. C. Correll, dissertation, University of Michigan, 1992.
35. EPR spectra of crystals, measured by W. R. Dunham and D. Gatti, distinguish the two- and three-electron reduced states of PDR, according to the presence or absence of the $g = 2.0$ signal. This technique established that PDR^{2-} was the major species in crystals reduced with NADH. However, quantitative measurement of the fraction of two-electron reduced species is complicated by orientation dependence and magnetic interactions. In solution, in the presence of excess NADH, the fully reduced protein, PDR^{3-}, is formed by intermolecular disproportionation reactions. The EPR spectra showed that this species was not the dominant form in crystals treated with NADH and used for x-ray measurements, either because intermolecular electron transfer is slow in the crystal or because the redox potential of the crystal suspension was above the midpoint potential for $FMNH^{\cdot}$:$FMNH^{-}$.
36. S. C. Andrews *et al.*, *FEBS Lett.* **302**, 247 (1992).
37. E. L. Neidle *et al.*, *J. Bacteriol.* **173**, 5385 (1991).
38. R. K. Wierenga, P. Terpstra, W. G. J. Hol, *J. Mol. Biol.* **187**, 101 (1986).
39. Superposition of FNR (*17*) and of *Anabaena 7120* Fd (*19*) on PDR provides a model for the dissociable Fd:FNR complex (*42*).
40. R. J. Gurbiel *et al.*, *Biochemistry* **28**, 4861 (1989).
41. W. Kabsch and C. Sander, *Biopolymers* **22**, 2577 (1983).
42. C. C. Correll, M. L. Ludwig, C. Bruns, P. A. Karplus, H. M. Holden, in preparation.
43. T. C. Terwilliger and D. Eisenberg, *Acta Crystallogr. Sect. A* **39**, 813 (1983).
44. G. Bricogne, in *Computational Crystallography*, D. Sayre, Ed. (Clarendon, Oxford, 1982), pp. 223–230.
45. W. A. Hendrickson, *Trans. Am. Crystallogr. Assoc.* **21**, 11 (1985).
46. C. Cambillau and E. Horjales, *J. Mol. Graph.* **5**, 174 (1987); T. A. Jones and S. Thirup, *EMBO J.* **5**, 819 (1986); T. A. Jones, J.-Y. Zou, S. W. Cowan, M. Kjeldgaard, *Acta Crystallogr. Sect. A* **47**, 110 (1991).
47. A. T. Brünger, *J. Mol. Biol.* **203**, 803 (1988); ———, A. Krukowski, J. W. Erickson, *Acta Crystallogr. Sect. A* **46**, 585 (1990); A. T. Brünger, *X-PLOR 2.1* (Yale University, New Haven, CT, 1990).
48. P. V. Luzzati, *Acta Crystallogr.* **5**, 802 (1952).
49. V. Massey and S. Ghisla, *Ann. N.Y. Acad. Sci.* **277**, 446 (1974); H. S. Shieh, S. Ghisla, L. K. Hanson, M. L. Ludwig, C. E. Nordman, *Biochemistry* **20**, 4766 (1981); M. F. Zipplies and H. A. Staab, in *Flavins and Flavoproteins*, R. C. Bray, P. C. Engel, S. G. Mayhew, Eds. (de Gruyter, Berlin, 1984), pp. 21–24.
50. Sequencing was performed by A. Vlahakis in P. Andrews' laboratory at the University of Michigan.
51. M. W. Hunkapillar, R. M. Hewick, W. J. Dreyer, L. E. Hood, *Methods Enzymol.* **91**, 399 (1983).
52. F. Brunel and J. Davidson, *J. Bacteriol.* **170**, 4924 (1988).
53. K. M. Flaherty, C. Deluca-Flaherty, D. B. McKay, *Nature* **346**, 623 (1990); W. Kabsch, H. G. Mannherz, D. Suck, E. F. Pai, K. C. Holmes, *ibid.* **347**, 37 (1990).
54. E. N. Baker and R. E. Hubbard, *Prog. Biophys. Mol. Biol.* **44**, 97 (1984); J. A. Ippolito, R. S. Alexander, D. W. Christianson, *J. Mol. Biol.* **215**, 457 (1990).
55. P. A. Karplus, K. A. Walsh, J. R. Herriott, *Biochemistry* **23**, 6576 (1984).
56. M. J. Simon *et al.*, *Gene*, in press.
57. Coordinates for PDR have been deposited in the Brookhaven Data Bank.
58. Supported by NIH grants GM 20877 (D.P.B.) and GM 16429 (M.L.L.). Coordinates for the structures of spinach NADP+ ferredoxin reductase and ferredoxin from *Anabaena 7120* were kindly provided by P. A. Karplus and H. M. Holden, respectively. Stereoviews were prepared with the program MAXIM, written by M. Rould. The area detector facility was maintained by the expertise of K. Shaw.

29 May 1992; accepted 4 November 1992